Theory of Control of the Spin-Photon Interface for Quantum Networks

Wang Yao, Ren-Bao Liu, and L. J. Sham

Department of Physics, University of California San Diego, La Jolla, California 92093-0319, USA

(Received 7 July 2004; published 13 July 2005)

A cavity coupling, a charged nanodot, and a fiber can act as a quantum interface, through which a stationary spin qubit and a flying photon qubit can be interconverted via a cavity-assisted Raman process. This Raman process can be made to generate or annihilate an arbitrarily shaped single-photon wave packet by pulse shaping the controlling laser field. This quantum interface forms the basis for many essential functions of a quantum network, including sending, receiving, transferring, swapping, and entangling qubits at distributed quantum nodes as well as a deterministic source and an efficient detector of a single-photon wave packet with arbitrarily specified shape and average photon number. Numerical study of errors from noise and system parameters on the operations shows high fidelity and robust tolerance.

DOI: 10.1103/PhysRevLett.95.030504 PACS numbers: 03.67.Lx, 42.50.Pq, 78.47.+p, 78.67.Hc

Quantum networks composed of local nodes and quantum channels are essential for quantum communication and desirable for scalable and distributed quantum computation [1,2]. Spins in quantum dots [3] or stable levels of atoms or ions [4,5] are good candidates for stationary qubits which can be locally stored and manipulated [6–8]. Photons in optical fibers or waveguides are ideal flying qubits for carrying quantum information between the local nodes. A quantum interface interconverting local and flying qubits is the key component of the quantum network. A recent experiment demonstrating entanglement between photon polarizations and states in an atom [9] represents a breakthrough in this direction. Another milestone toward quantum networks is the proposal of Cirac *et al.* based on cavity-assisted Raman processes [10], which employs time-symmetrical carrier pulses and mutually time-reversed operations at two nodes to transfer a qubit state from one node to another.

This Letter proposes a general control scheme of a spin-photon quantum interface, of which the time symmetric scheme of [10] and the adiabatic scheme of [11] form special and approximate cases. It also presents the operation and error analyses of a semiconductor quantum dot–waveguide interface coupled by a cavity, a basis for a solid-state quantum network.

We note that the state-transfer process proposed in Ref. [10] can be separated into two steps: the sending operation at one node which maps a stationary qubit into a flying qubit by the evolution $[C_g|g\rangle + C_e|e\rangle] \otimes |\mathrm{vac}\rangle \rightarrow |g\rangle \otimes [C_g|\mathrm{vac}\rangle + C_e|\alpha(t)\rangle]$ and the receiving operation at another node which maps the flying qubit into a stationary one, where $|g\rangle$ and $|e\rangle$ are the stationary qubit states and the flying qubit is represented by the vacuum state $|\mathrm{vac}\rangle$ and a single-photon state with wave packet $\alpha(t)$. We will show that both the sending and receiving processes can be independently controlled by shaping the laser pulses. Two aspects of the process are controllable: the production of an arbitrarily shaped pulse provided that it is sufficiently smooth and the operation of the Raman process as a partial cycle, in which the initial state $|e\rangle \otimes |\mathrm{vac}\rangle$ is mapped into an entangled state $\cos\theta|e\rangle \otimes |\mathrm{vac}\rangle + \sin\theta|g\rangle \otimes |\alpha(t)\rangle$ for any $\theta \in [0, \pi/2]$.

With such controllability in hand, this quantum interface can accomplish many essential functions of a quantum network: (i) It can send a flying quantum state and can also function as a deterministic source of single photons with arbitrary pulse shape and controllable photon number. (ii) It can receive a flying quantum state, being an efficient single-photon detector provided that the incoming photon pulse shape is known. (iii) The sending and receiving processes combined transfer a state from one node to another. (iv) An incoming flying qubit may be swapped with a stationary qubit which enables the swap of two remote qubits. (v) An entangled state of the stationary and flying qubits is produced in a partial Raman cycle. (vi) Two stationary qubits separated by a large distance are entangled when the photon state generated by the partial Raman cycle is mapped into a stationary qubit. The extension to a network of these nodes connecting small optical computers of spin qubits in dots [6–8] is straightforward and will be published later.

The basis for the physical implementation of our proposal of a node is formed by a substantial list of recent experimental advances on optical manipulation of excitons in single nanodots [12], nanodot-microsphere coupling [13], cavity-fiber coupling [14], fabrication of high-quality microcavities and waveguides, both on semiconductor surfaces [14] and in photonic crystals [15,16], and especially the very recent findings of vacuum Rabi splitting of nanodots embedded in such cavities [17,18]. The duration of a typical operation in the node is shown below to be of the order 100 ps, consistent with the theoretical estimates of optical operations on spin qubits in dots for network purposes. The speed and pulse shaping may well be within the capability of the existing ultrafast optics.

The prototype quantum interface is made up of a high-Q microcavity coupling, a quantum dot, and a waveguide (e.g., a fiber), such as is shown in Fig. 1(a). Lowering of

the Q of the cavity due to the strong coupling with the waveguide is part of the process and has no deleterious effect on the quantum operation. The detailed optical process is depicted in Fig. 1(b). The qubit is represented by the two spin states $|g\rangle$ and $|e\rangle$ which have split energies ω_g and ω_e in a static magnetic field normal to the optical axis of the dot. The lowest two optically excited states are two spin states of a heavy hole plus a singlet of two electrons, known as trion states $|t\rangle$ and $|\bar{t}\rangle$, with energies ω_t and $\omega_{\bar{t}}$ respectively. The linear optical polarizations are chosen [19] such that the cavity mode of frequency ω_c couples with strength g_{cav} only to the transitions $|g\rangle \rightarrow |t\rangle$ and $|e\rangle \rightarrow |\bar{t}\rangle$, and the controlling laser of central frequency ω_L and complex Rabi frequency $\Omega(t)$ couples only to the cross transitions $|g\rangle \rightarrow |\bar{t}\rangle$ and $|e\rangle \rightarrow |t\rangle$. The laser light and cavity mode satisfy the resonance condition: $\omega_L + \omega_e = \omega_c + \omega_g = \omega_t$. By the Zeeman splitting and the selection rules, the trion state $|\bar{t}\rangle$ is off resonant to the laser light and the cavity mode (shown by dashed lines in the figure). The cavity mode is coupled to the waveguide continuum by the coupling constant κ.

At a sending node, the Raman process consists in first the laser field resonantly exciting the spin state $|e, 0\rangle$ to the trion state $|t, 0\rangle$, then the trion state resonantly coupled to the cavity state $|g, 1\rangle$, which finally is rotated to the spin state $|g, 0\rangle$ forming a photon wave packet in the waveguide. The receiving node is just the time-reversed process. Undesirable dynamics involving the state $|\bar{t}\rangle$ is eliminated by making the Zeeman splitting sufficiently larger than the cavity-dot coupling and the Rabi frequency. The resultant optical process is the cavity-assisted resonant Raman process in a Λ-type three-level system shown in Fig. 1(c). Then for any shape of the single-photon wave packet in the waveguide, an analytical solution of the pulse shape of the laser field may be found. With this analytically obtained

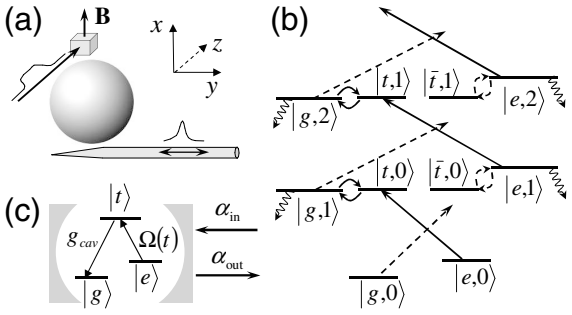

FIG. 1. (a) A high-Q microsphere coupling, a "tapered" waveguide, and a doped quantum dot. (b) The level diagram and optical process. In $|s, n\rangle$, $s = g, e, t$, or $\bar{t}$ denotes an electronic state in the dot and n denotes the number of photons in the single cavity mode. Straight, curved, and wavy arrows represent the laser excitation, dot-cavity coupling, and cavity-fiber tunneling, respectively. The resonant and off-resonant processes are represented by solid and dashed lines, respectively. (c) The simplified cavity-assisted Raman process.

laser pulse shape as the controlling input, numerical calculations including the nonresonant transitions and realistic decoherence have been performed and high fidelity of desired operations at the quantum interface is demonstrated.

We first present the analytical solution of the laser pulse for the controlled Raman transition converting a spin qubit state $[C_g|g, 0\rangle + C_e|e, 0\rangle] \otimes |\mathrm{vac}\rangle$ to a flying photon state $|g, 0\rangle \otimes [C_g|\mathrm{vac}\rangle + C_e|\alpha(t)\rangle]$. Throughout the optical process in the simplified system in Fig. 1(c), the state $|g, 0\rangle|\mathrm{vac}\rangle$ does not mix with the subspace with basis $\{|e, 0\rangle|\mathrm{vac}\rangle, |t, 0\rangle|\mathrm{vac}\rangle, |g, 1\rangle|\mathrm{vac}\rangle, |g, 0\rangle|\omega\rangle\}$, where $|\omega\rangle$ denotes the one-photon Fock state of the waveguide mode with frequency ω. Hence, the state of the system at any time has the form $C_g|g, 0\rangle|\mathrm{vac}\rangle + C_e|\Psi^e(t)\rangle$, where

$$|\Psi^e(t)\rangle = \beta_e(t)|e, 0\rangle|\mathrm{vac}\rangle + \beta_t(t)|t, 0\rangle|\mathrm{vac}\rangle + \beta_c(t)|g, 1\rangle|\mathrm{vac}\rangle + \int_0^\infty d\omega\, \alpha_\omega(t)|g, 0\rangle|\omega\rangle.$$

Within the Weisskopf-Wigner approximation, the equation of motion for the resonant Raman process in the interaction picture can be derived as

$$\dot{\beta}_e = -\Omega^*(t)\beta_t/2, \tag{1a}$$

$$\dot{\beta}_t = +\Omega(t)\beta_e/2 + g^*_{\mathrm{cav}}\beta_c, \tag{1b}$$

$$\dot{\beta}_c = -\gamma\beta_c/2 - g_{\mathrm{cav}}\beta_t - \sqrt{2\pi}\kappa^*\alpha_{\mathrm{in}}(t) \tag{1c}$$

$$= +\gamma\beta_c/2 - g_{\mathrm{cav}}\beta_t - \sqrt{2\pi}\kappa^*\alpha_{\mathrm{out}}(t), \tag{1d}$$

where $\gamma \equiv 2\pi|\kappa|^2$ gives the cavity damping rate, and $\alpha_{\mathrm{in}}(t) \equiv \int d\omega\, \alpha_\omega(t_0)e^{-i(\omega-\omega_c)t}/\sqrt{2\pi}$ with $t_0 \rightarrow -\infty$ and $\alpha_{\mathrm{out}}(t) \equiv \int d\omega\, \alpha_\omega(t_1)e^{-i(\omega-\omega_c)t}/\sqrt{2\pi}$ with $t_1 \rightarrow +\infty$ are the incoming and outgoing pulse of the photon in the quantum channel, respectively. The quantum fluctuation caused by the quantum channel is on the order of $\gamma/\omega_c \ll 1$ and, thus, the Weisskopf-Wigner approximation is well justified here, though it can be shown to be unnecessary.

In the process of mapping the spin qubit to the photon qubit, there is no incoming photon, so the initial conditions are $\alpha_{\mathrm{in}}(t) = 0$, $\beta_c(t_0) = 0$, $\beta_e(t_0) = 1$, and $\beta_t(t_0) = 0$. In the driven quantum evolution, the amplitude is coherently transferred through the pathway: $\beta_e \xrightarrow{\Omega} \beta_t \xrightarrow{g_{\mathrm{cav}}} \beta_c \xrightarrow{\kappa} \alpha_\omega$. Three features make the design of the evolution possible: (i) From Eqs. (1c) and (1d), the cavity mode coefficient β_c is a direct map of the photon pulse shape, $\beta_c = \tilde{\alpha}_{\mathrm{out}} \sin\theta/(\sqrt{2\pi}\kappa)$, where the normalized photon pulse shape $\tilde{\alpha}_{\mathrm{out}}$ and the average photon fraction $\sin^2\theta$ may be arbitrary specified, and the trion state coefficient is given by $\beta_t = (-\dot{\beta}_c - \gamma\beta_c/2)/g_{\mathrm{cav}}$. (ii) The amplitude of β_e is given by the normalization condition and its phase can be expressed from Eq. (1) as

$$\frac{d}{dt}\arg(\beta_e) = \frac{|\dot{\beta}_c + \gamma\beta_c/2|^2}{|g_{\rm cav}|^2|\beta_e|^2}\frac{d}{dt}\arg(\dot{\beta}_c + \gamma\beta_c/2) - |\beta_e|^{-2}|\beta_c|^2\frac{d}{dt}\arg(\beta_c). \quad (2)$$

(iii) The controlling laser pulse $\Omega(t)$ can thus be expressed in terms of the cavity mode β_c and the spin β_e analytically from Eq. (1b),

$$\frac{\Omega}{2} = -\frac{g^*_{\rm cav}\beta_c}{\beta_e} - \frac{\ddot{\beta}_c + \gamma\dot{\beta}_c/2}{g_{\rm cav}\beta_e}. \quad (3)$$

At the remote future $t_1 \to +\infty$, the photon emission process is completed, i.e., $\beta_c(t_1) = \dot{\beta}_c(t_1) = 0$, so $\beta_e(t_1) = e^{i\phi}\cos\theta$ with the controllable phase ϕ independent of the initial superposition [see Eq. (2)].

When the full Raman transition is completed, $\theta = \pi/2$ and $\beta_e(t_1) = 0$. Thus, the spin qubit is mapped onto the flying qubit by the transformation

$$(C_g|g\rangle + C_e|e\rangle) \otimes |\text{vac}\rangle \xrightarrow{\Omega} |g\rangle \otimes [C_g|\text{vac}\rangle + C_e|\tilde{\alpha}_{\rm out}\rangle]. \quad (4)$$

The mapping operation also functions as a deterministic generation of a single-photon wave packet with any desired pulse shape $\tilde{\alpha}_{\rm out}$ and average photon number $|C_e|^2$.

The Raman process at the receiving node is basically the time reversal of the above sending process. The incoming photon pulse $\alpha_{\rm in}(t)$ can be arbitrarily specified provided that it is smooth enough, and the photon is absorbed without reflection. As the spin state converted from the photon state can be read out nondestructively [20], the receiving node can also act as an efficient photon detector which measures the photon number state given the photon pulse shape is known.

The Raman cycle at the sending node can also be controlled such that $\theta < \pi/2$. The initial state $|e\rangle \otimes |\text{vac}\rangle$ is transformed into an entangled state of the stationary spin and the flying photon and the mapping process at the receiving node will just produce a nonlocally entangled state of the two spins by the transformation

$$|e\rangle_1|g\rangle_2 \otimes |\text{vac}\rangle \xrightarrow{\Omega_1} e^{i\phi}\cos\theta|e\rangle_1|g\rangle_2 \otimes |\text{vac}\rangle + \sin\theta|g\rangle_1|g\rangle_2 \otimes |\tilde{\alpha}_{\rm out}\rangle \xrightarrow{\Omega_2} [e^{i\phi}\cos\theta|e\rangle_1|g\rangle_2 + \sin\theta|g\rangle_1|e\rangle_2] \otimes |\text{vac}\rangle. \quad (5)$$

The entanglement entropy $-\cos^2\theta\log_2\cos^2\theta - \sin^2\theta\log_2\sin^2\theta$ can be set any value between 0 and 1 depending on the rotating angle θ. Although Eqs. (1c) and (1d) contain terms which yield exponential dependence on time, they are time reversible with each other. Thus, contrary to the usual view of a continuum being a source of dissipation and decoherence, the controlled general swap between a spin qubit and a photon wave packet qubit is actually a reversible quantum operation. It follows that, by proper design of the driven term $\Omega(t)$ at each node, entanglement operation between two distant spin qubits mediated by a photon continuum is possible.

The error of the quantum operations described above is estimated in terms of fidelity by numerical simulations including the undesired nonresonant dynamics and unavoidable decoherence. The main source of decoherence is the trion decay by spontaneous emission and the cavity mode leakage other than the dynamics accounted above. The fiber loss and the spin relaxation are negligible on the time scale of 100 ps and the distance scale of 1 cm of relevance here. The trion decay rate, based on experiment [21], is set at $\Gamma = 3$ μeV, and the intrinsic loss rate of a high-Q cavity excluding coupling to the dot and the fiber is assumed to be $\gamma_0 = 0.1$ μeV (corresponding to a Q factor $\sim 10^7$). The cavity-fiber tunneling rate is chosen to be $\gamma = 0.2$ meV and the dot-cavity coupling constant $g_{\rm cav} = 0.1$ meV. The remaining sources of error are the nonresonant excitation of the multiphoton states and AC Stark shift of the energy levels. The latter induces a deterministic phase drift between $|g\rangle$ and $|e\rangle$, which is independent of the coefficients $C_{g(e)}$ as the two excitation pathways starting, respectively, from $|g\rangle$ and $|e\rangle$ are independent of each other [see Fig. 1(b)], and thus can be compensated by a single-qubit operation. Leakage out of the qubit subspace by the nonresonant excitation to multiphoton states is greatly suppressed by a 1 meV Zeeman splitting (at less than 10 T magnetic field for InAs dots), which is much larger than the Rabi frequency and the cavity-dot coupling.

We present in Fig. 2 the simulation result of mapping a spin state to a flying photon wave packet with the pulse shape targeted as a superposition of two sech functions as $\alpha^{\rm ideal}_{\rm out}(t) = \text{sech}(\gamma t/6 + 5) + 0.5\,\text{sech}(\gamma t/6 - 5)$, with normalization understood. The fidelity of the photon pulse generation $|\langle\alpha^{\rm ideal}_{\rm out}|\alpha_{\rm out}\rangle| \approx 0.9912$. Because of the nonadiabatic optical pumping and dot-cavity coupling, the

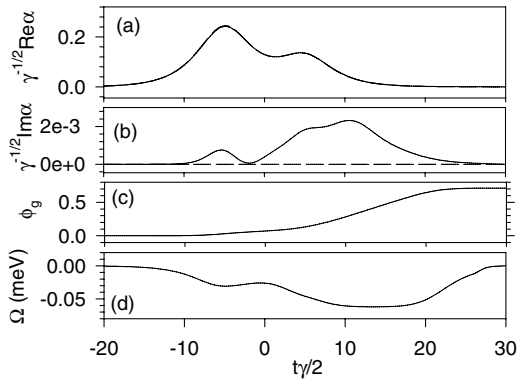

FIG. 2. Generation of a double sech photon pulse. (a) Real part of the dimensionless amplitude of the simulated photon pulse (solid line) as a function of the dimensionless time $\gamma t/2$. The deviation from the target pulse is not visible. (b) Imaginary part of the simulated pulse (solid line) and the target pulse (dashed line). (c) Phase drift of the state $|g, 0\rangle$. (d) Rabi frequency of the control laser.

TABLE I. Merits of entanglement creation with various photon pulse shape, normalization understood. $g_{\mathrm{cav}}^{1,2} = 0.1$ meV and $\gamma^{1,2} = 0.2$ meV.

$\alpha(t)$	$\mathrm{sech}(\frac{\gamma t}{6})$	$\exp(-\frac{\gamma^2 t^2}{128})$	$\frac{1+\tanh(\gamma t/8)}{\cosh(\gamma t/6)} + \frac{1-\tanh(\gamma t/8)}{\exp(\gamma^2 t^2/128)}$
Fidelity	0.9912	0.9908	0.9906
$E(\rho_{\mathrm{qubit}})$	0.9995	0.9995	0.9994
P_{leak}	0.0173	0.0182	0.0184

whole mapping process can be completed within 300 ps. The simulation of the photon absorption process shows an overall fidelity greater than 0.99 as well.

We have compared the merits among different target photon pulse shapes for various network operations. The fast diminishing tails of the Gaussian pulse tend to require a higher peak value of $\Omega(t)$ than the exponential tails of the sech pulse and, thus, cause more nonresonant excitations (i.e., undesired dynamics) than the latter. On the other hand, deviation from the target shape at the tail region of the photon pulse has a negligible effect on the fidelity of interface operations as compared to nonresonant excitation; thus tuning down $\Omega(t)$ at the tail region can make the Gaussian pulse more efficient for achieving fidelity. Table I shows the results of a comparative study of the merits of the photon pulse in the sech shape, the Gaussian, and an asymmetric shape with sech on the rise and Gaussian on the fall, mediating entanglement of two spin qubits to the Bell state $e^{i\phi}|g\rangle_1|e\rangle_2 + |e\rangle_1|g\rangle_2$. The merits calculated are the fidelity, the entanglement of formation $E(\rho_{\mathrm{qubit}})$ in the subspace of the two spin qubits, and the probability of leakage out of this subspace, P_{leak}.

In the preceding analysis, exact knowledge of the coupling strengths, g_{cav}, γ, and $\Omega(t)$, is assumed. Table II shows the effect of the unknown errors in the various parameters on the fidelity of entanglement to $e^{i\phi}|g\rangle_1|e\rangle_2 + |e\rangle_1|g\rangle_2$ and transfer of the $|g\rangle + |e\rangle$ state both with the photon pulse shape $\mathrm{sech}(\frac{\gamma t}{6})$. Our system shows a surprising robustness: 10% errors on g_{cav}, γ, or $|\Omega(t)|$ reduce the fidelity by less than 1%. $\Omega(t)$ can also have unknown phase error due to laser fluctuation which can be considered static in the time scale of our operation. What matters in two node operations is the relative phase between $\Omega_1(t)$ and $\Omega_2(t-\tau)$ where τ is the propagation delay. This property enables us to protect network function by a delayed phase locking of the control field at the two nodes. Laser phase fluctuation will then induce no effect on the state transfer or swap and the entanglement creation scheme.

In summary, controllable and high-fidelity quantum operations for stationary spin and flying photon qubits, based on a cavity-assisted Raman process, are shown to be theoretically feasible with solid-state elements including charged quantum dots, microspheres (or microcavities), and waveguides (or fibers). The control scheme presented

TABLE II. Effect of errors in coupling parameters on the fidelity of entanglement and of state transfer.

	no error	10% g error	10% γ error	10% $\Omega(t)$ error
Entangle	0.9912	0.9872	0.9894	0.9862
Transfer	0.9901	0.9870	0.9891	0.9879

may be applied to systems in very different parameter regimes, e.g., ions trapped in cavity [22], with the requirement of node identity removed, greatly saving the resources to implement the quantum network. The exact solution also allows learning studies on the system parameters while the intrinsic robustness against unknown parameter errors paves the way for further exploration of quantum feedback control [23,24] for this system.

This Work was supported by NSF DMR-0099572, ARDA/ARO DAAD19-02-1-0183, and QuIST/AFOSR F49620-01-1-0497.

[1] J. I. Cirac, A. K. Ekert, S. F. Huelga, and C. Macchiavello, Phys. Rev. A **59**, 4249 (1999).
[2] D. DiVincenzo, Fortschr. Phys. **48**, 771 (2000).
[3] D. Loss and D. P. DiVincenzo, Phys. Rev. A **57**, 120 (1998).
[4] C. Monroe *et al.*, Phys. Rev. Lett. **75**, 4714 (1995).
[5] J. I. Cirac and P. Zoller, Phys. Rev. Lett. **74**, 4091 (1995).
[6] A. Imamoğlu *et al.*, Phys. Rev. Lett. **83**, 4204 (1999).
[7] C. Piermarocchi, P. Chen, L. J. Sham, and D. G. Steel, Phys. Rev. Lett. **89**, 167402 (2002).
[8] P. Chen *et al.*, Phys. Rev. B **69**, 075320 (2004).
[9] B. B. Blinov, D. L. Moehring, L.-M. Duan, and C. Monroe, Nature (London) **428**, 153 (2004).
[10] J. I. Cirac, P. Zoller, H. J. Kimble, and H. Mabuchi, Phys. Rev. Lett. **78**, 3221 (1997).
[11] L.-M. Duan, A. Kuzmich, and H. J. Kimble, Phys. Rev. A **67**, 032305 (2003).
[12] X. Li *et al.*, Science **301**, 809 (2003).
[13] X. D. Fan *et al.*, Opt. Lett. **25**, 1600 (2000).
[14] K. J. Vahala, Nature (London) **424**, 839 (2003).
[15] A. Scherer *et al.*, IEEE Trans. Nanotechnol. **1**, 4 (2002).
[16] Y. Akahane, T. Asano, B.-S. Song, and S. Noda, Nature (London) **425**, 944 (2003).
[17] J. P. Reithmaier *et al.*, Nature (London) **432**, 197 (2004).
[18] T. Yoshie *et al.*, Nature (London) **432**, 200 (2004).
[19] W. Yao, R. Liu, and L. J. Sham, Phys. Rev. Lett. **92**, 217402 (2004).
[20] R. Liu, W. Yao, and L. J. Sham cond-mat/0408148 [Phys. Rev. B (to be published)].
[21] M. Bayer and A. Forchel, Phys. Rev. B **65**, 041308 (2002).
[22] M. Keller *et al.*, Nature (London) **431**, 1075 (2004).
[23] H. M. Wiseman and G. J. Milburn, Phys. Rev. Lett. **70**, 548 (1993).
[24] H. Rabitz, R. de Vivie-Riedle, M. Motzkus, and K. Kompa, Science **288**, 824 (2000).